Chapter

Low-Profile Metamaterial-Based Adaptative Beamforming Techniques

Chung-Tse Michael Wu and Pai-Yen Chen

Abstract

In this chapter, we will review recent research advances on beamforming and spatial multiplexing techniques using reconfigurable metamaterials (MTMs) and metasurfaces. This chapter starts by discussing basic principles and practical applications of transmission line-based metamaterials and planar metasurfaces, followed by their active versions that enable novel smart antennas with beam steering and beamshaping functions. We include detailed descriptions of their practical realizations and the integration with circuits and the radio-frequency (RF) frontend, which are used to adaptively and dynamically manipulate electromagnetic radiation. We summarize the state-of-the-art MTM/metasurface-based beamforming techniques and provide a critical comparison for their uses in the RF-to-millimeter-wave range in terms of cost, reconfigurability, system integratability and radiation properties. These techniques are expected to pave the way for the massive deployment of communication, radar, remote sensing and medical and security imaging systems.

Keywords: beamforming, composite right/left-handed transmission lines, leaky wave antennas, metamaterials, metasurfaces

1. Introduction

Metamaterials (MTMs) are artificial composite structures having anomalous electromagnetic properties that are not found in naturally occurring materials. Examples include the negative refractive index [1–3] and the terahertz (THz) and optical magnetism [4]. The word "meta" is sourced from a Greek word that means beyond or after. Metamaterials are generally constituted by arrays of subwavelength inclusions with induced electric and/or magnetic dipole moment, such as magnetodielectric spheres. The periodicity between neighboring inclusions is much smaller than the wavelength of impinging light and dominant Bloch modes. The first 3D MTM was realized in the microwave regime using arrays of metal wires and split-ring resonators (SRRs) [2–4]. For the first time, this structure has been demonstrated to exhibit a simultaneously negative permittivity and permeability, resulting in a negative index of refraction. A negative-index or double-negative (DNG) MTM is generally named as a "left-handed" medium, which supports the electromagnetic wave propagation with an exotic negative phase velocity and negative refraction. In a left-handed medium, the Snell's law is inverted and evanescent

waves could be amplified to make a "perfect lens" that enables sub-diffraction imaging [2, 3].

The left-handed propagation properties can also be realized using the printed-circuit transmission line (TL), which eases the fabrication complexity of metamaterials at high frequencies [5–7]. The TL-based MTMs, also termed as composite right/left-handed transmission lines (CRLH-TLs), have gained popularity in RF and microwave bands, owning to their low cost, compactness and compatibility with the printed circuit technology. Moreover, the TL structures based on non-resonant lumped elements can provide broader bandwidth and lower power dissipations compared with those bulky metamaterials composed of 3D arrays of resonant inclusions. The planar TL MTMs also allow the integration with active and/or passive tuning components, such as varactors or field-effect transistors (FETs), for making adaptive and spectral/spatial-reconfigurable electromagnetic responses. The TL MTMs therefore provide a useful platform for observing the phenomena of negative material properties and for reaching various metamaterial-enabled applications. The exotic guided- and leaky-wave properties in the CRLH-TL medium, associated with the negative phase velocity, have been proposed to realize different kinds of planar microwave circuit blocks, such as the multi-band and enhanced bandwidth power combiners/splitters, resonators, couplers [8], phase shifters [9], bandpass filters [10] and subwavelength focusing devices [11, 12]. Furthermore, the fast wave and dual RH-LH characteristics existing in the periodic CRLH-TL structures have been exploited to excite leaky wave radiations and to implement one-dimensional (1D) and two-dimensional (2D) leaky-wave antennas (LWAs) with superior radiation properties and tunability [13–16]. These metamaterial-based leaky-wave antennas can not only be compact and low-profile, but also achieve a directive beam that can be steered from backfire, broadside to endfire. Such a wide-angle beam scanning is not available in conventional uniform or periodic leaky-wave antennas, which require complex and narrow-band feeding networks [17]. Most interestingly, by loading an MTM LWA with tuning elements, such as p-i-n or varactor switching diodes [18], it is possible to achieve fast and frequency-locked beamscanning, which is by the external biasing circuitry. Consequently, the beam scanning can function properly at a specific operating frequency, which is of great interest for the spatial channelizing in the modern communication systems.

RF and microwave beamforming techniques have drawn intensive research interest in 5G wireless communication [i.e., spatial multiplexing multiple access (SDMA) and space shift keying (SSK)], microwave imaging and radar for the directional and reconfigurable RF signal transmission or reception. Here, we note that the beamforming technique can be used at both the transmitting and receiving ends to achieve spatial selectivity. Conventional beamforming systems are generally based on mechanically steered antennas, with the assistance of motors and gimbals, which, however have several disadvantages, such as relatively large size and weight, as well as a slow beam scanning rate. Alternatively, phased arrays consisting of multiple active antennas are also commonly used to launch electromagnetic waves to a particular direction, by means of properly phasing the wavefront of individual antennas to cause constructive or destructive interference. However, phased arrays are composed of lots of radiating elements and at least one stage of amplifier and phase shifter, and are expensive to purchase due to their technical complexity.

In this chapter, we will present an overview of TL-based MTMs and their applications in smart and reconfigurable antennas. We will review different kinds of recently developed planar MTM and metasurface antennas with beamforming and beamshaping functions, as well as their practical applications. We begin by discussing the background of TL MTMs that lead to the development of printed

LWAs, and then introduce other state-of-the-art surface antenna technologies, such as the holographic antennas based on metasurfaces.

2. Transmission line metamaterials

Figure 1a illustrates the unit cell of a conventional lossless right-handed (RH) transmission line (TL) model, where the equivalent circuit contains series inductance (L_R) and shunt capacitance (C_R). The unit cell is assumed to represent a small section of the transmission line, much less than one quarter of the guided wavelength. The equivalent MTM constitutive parameters, such as permittivity and permeability can be obtained by mapping the Maxwell's equation onto the telegrapher's Equation [19]. As such, the propagation constant (β) can be derived in terms of the series impedance (Z') and shunt admittance (Y'), in which $Z' = j\omega L_R$ and $Y' = j\omega C_R$ [5]:

$$j\beta = \sqrt{Z'Y'} = j\omega\sqrt{L_R C_R} \tag{1}$$

From (1), we obtain a dispersion relationship that is linearly proportional to the frequency, as illustrated in (2) and **Figure 1b**:

$$\beta_{RH} = \omega\sqrt{L_R C_R} \tag{2}$$

On the other hand, a left-handed (LH) TL can be obtained by interchanging the inductor and capacitor in the RH TL unit cell. As illustrated in **Figure 2a**, the series impedance now is changed to a capacitance, whereas the shunt admittance becomes an inductance. Using a similar derivation as shown in (1), by replacing Z' with $1/j\omega C_L$ and Y' with $1/j\omega L_L$, the propagation constant can be expressed as:

$$\beta_{LH} = -\frac{1}{\omega\sqrt{L_L C_L}} \tag{3}$$

The negative sign of the propagation constant indicates the phase velocity is opposite to the direction of that for a RH-TL, which is governed by the "left-hand" rule. This left-handed (LH) TL is regarded as a kind of planar MTM, as it has novel negative-phase-velocity property that can only be artificially engineered. The corresponding dispersion diagram of such left-handed transmission line is shown in **Figure 2b**.
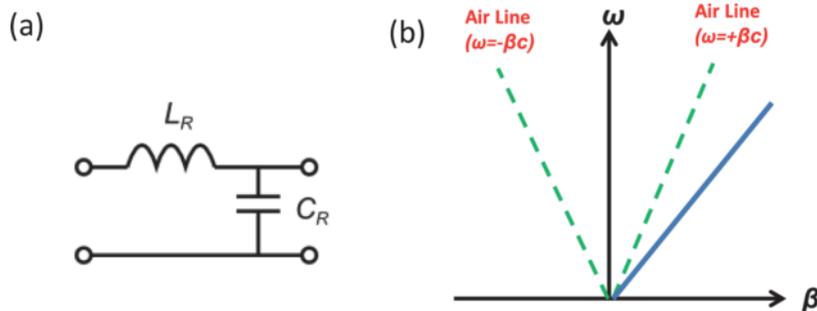
Figure 1.
(a) Unit cell and (b) dispersion diagram of a right-handed (RH)-TL model; the dashed lines represent the air lines.

(a)

(b)
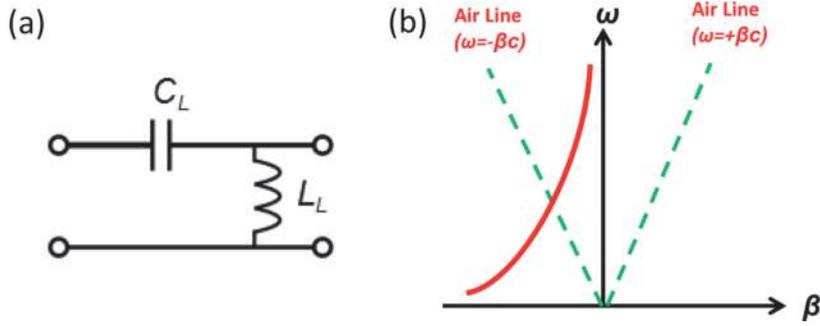
Figure 2.
(a) Unit cell and (b) dispersion diagram of a left-handed transmission line model; the dashed lines represent the air lines.

(a)

(b)
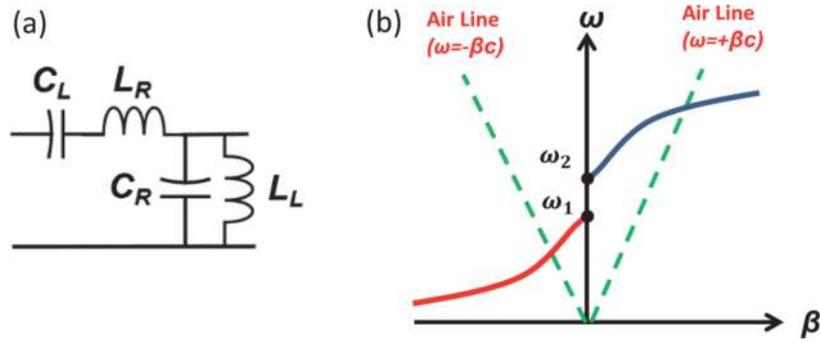
Figure 3.
(a) Unit cell and (b) dispersion diagram of a composite right/left-handed (CRLH)-TL model; the dashed lines represent the air lines.

Unlike the conventional case, the dispersion of a LH-TL is nonlinear and is always negative; the dashed lines represent the air lines. Nevertheless, in practice, due to the inevitable parasitic effect of host medium, it is rather difficult to realize the perfect left-handed TL MTMs. Indeed, the ordinary RH wave propagation is supported at higher frequencies. Therefore, a more generalized circuit model as shown in **Figure 3a** must be adopted to accommodate both RH and LH propagations. This configuration is the so-called composite right/left-handed transmission line (CRLH-TL). The dispersion relation can be derived using the same procedure by letting $Z' = j\omega L_R + 1/j\omega C_L$ and $Y' = j\omega C_R + 1/j\omega L_L$. After some mathematical manipulations, the propagation constant can be written as:

$$\beta_{CRLH} = s(\omega)\sqrt{\omega^2 L_R C_R + \frac{1}{\omega^2 L_L C_L} - \left[\frac{L_R}{L_L} + \frac{C_R}{C_L}\right]} \tag{4}$$

where

$$s(\omega) = \begin{cases} -1, \omega < \omega_2 = min\left\{\dfrac{1}{\sqrt{L_R C_L}}, \dfrac{1}{\sqrt{L_L C_R}}\right\} \\[2ex] 1, \omega > \omega_1 = max\left\{\dfrac{1}{\sqrt{L_R C_L}}, \dfrac{1}{\sqrt{L_L C_R}}\right\} \end{cases} \tag{5}$$

Figure 3b plots the corresponding dispersion curve, from which we can observe that the CRLH-TL can support both of the LH mode ($\beta < 0$) in the low frequency region and the RH mode ($\beta > 0$) in the high frequency region. Depending on the

operating frequency, CRLH-TLs can have different LH or RH characteristics. In addition, if we define two air lines that have a slope of speed of light c, we can divide the dispersion diagram into two regions. The region sandwiched by the two air lines is called the *fast wave* region, as the phase velocity ($v_p = \omega/\beta$) is greater than c. On the other hand, the rest is defined as the *slow wave* region as v_p is slower than c. CRLH-TLs behave differently in these two regions. As will be shown in the next section, CRLH-TLs will radiate in the fast wave region, corresponding to a "leaky" mode, which is necessary for a LWA. On the other hand, when operated in the slow wave region, corresponding to a "guided" mode, CRLH-TLs behave like waveguiding structures with ignorable radiation loss. The dual RH/LH and guided-to-leaky wave characteristics make CRLH-TLs fascinating structures offering significantly more flexibility in the design of guided-wave and radiated-wave microwave components.

Figure 4 shows the comparison of dispersion characteristics between a CRLH-TL and a conventional RH-TL. As discussed in the previous section, the dispersion region can be divided into radiation (leaky wave) and guided wave regions. Moreover, depending on the polarity of the propagation constant β, the dispersion diagram can be categorized to right-handed ($\beta > 0$) and left-handed ($\beta < 0$) regions. A conventional RH-TL will lie in the RH guided region, as it has a positive β ($\beta > \omega/c$ or $v_p < c$) and will not radiate. On the other hand, the dispersion curve of CRLH-TL continues across all the four regions in the dispersion diagram, which are LH guided, LH radiated, RH guided and RH radiated wave regions. As a result, CRLH-TL structures provide flexibility to tailor the electromagnetics responses at will. The band gap at $\beta = 0$ ($v_p \to \infty$) will disappear, if the following condition is satisfied:

$$\sqrt{\frac{L_R}{C_R}} = \sqrt{\frac{L_L}{C_L}} \text{ or } L_R C_L = L_L C_R \tag{6}$$

We call this a "balanced" condition for a CRLH-TL. A balanced CRLH-TL does not have a band gap and therefore has a smooth transition at the center frequency where the propagation constant is zero. This property is especially useful when it operates as a leaky wave antenna, as it allows a continuous frequency-dependent beam-scanning capability.

If the CRLH-TL operates in the radiated or fast wave region with $\beta < \omega/c$ or $v_p > c$, it will leak out power to the free space as the wave travels along the transmission line. Therefore, a leaky wave antenna is sometimes referred as a fast-wave traveling wave antenna.
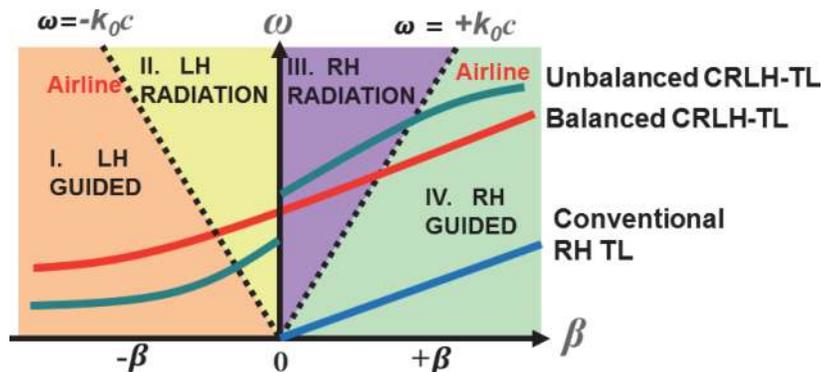
Figure 4.
Dispersion diagram of a composite right/left-handed transmission line model.

To further explain the leaky-wave characteristics, **Figure 5** illustrates the relationship between the vertical wavenumber k_z, the free space wavenumber k_0 and the modal propagation (phase) constant inside the wave guiding structure β_x. Here k_z can be expressed as:

$$k_z = \sqrt{k_0^2 - \beta_x^2} \tag{7}$$

When the wave propagates through the leaky wave structure with a complex wavenumber $\beta_x - j\alpha$, the fields outside the structure have the general form [17]:

$$\varphi(x,z) = \varphi_0\left(e^{-\alpha z}e^{-j\beta_x x}\right)e^{-jk_z z} \tag{8}$$

The attenuation constant $\alpha = \alpha_{loss} + \alpha_{rad}$, where α_{loss} is due to the material (dielectric and conduction) loss inside the guiding structure and α_{rad} is due to the radiative energy leakage (leakage rate). Therefore, one can observe that if k_z is a real number, that is, $k_0 > \beta_x$, the wave can propagate along the z-direction and hence the leakage radiation occurs. This is consistent with the aforementioned statement that when the CRLH-TL operates in the fast wave region ($v_p = \omega/\beta_x > c = \omega/k_0$), the propagating wave will be coupled into the free-space radiation, with a real value of k_z. On the other hand, if k_z is imaginary, the wave will decay exponentially along the z-direction, which results in an evanescent mode of the field.
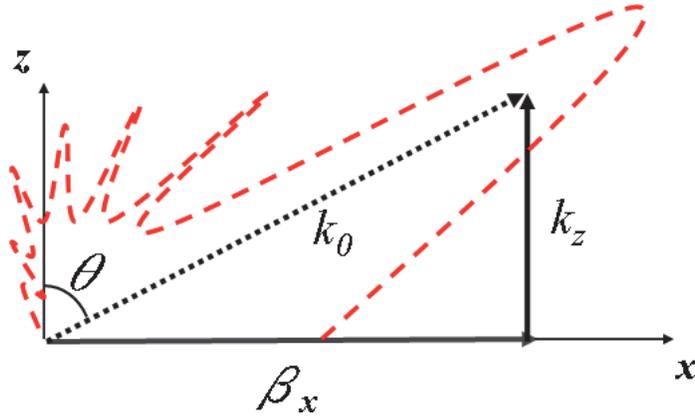
Figure 5.
Illustration of radiation phenomenon.
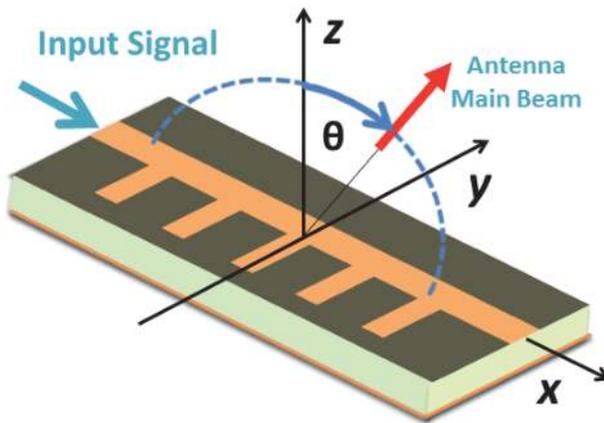
Figure 6.
1D CRLH leaky wave antenna (LWA).

From the vectorial relation shown in **Figure 5**, the direction of the main beam of radiation can be determined as

$$\theta_{MB} = \sin^{-1}\left(\frac{\beta_x}{k_0}\right) \tag{9}$$

Eq. (9) is approximately valid in many practical antennas, provided that $\alpha \ll \beta_x$. It can be known from **Figure 6** that since β_x is a function of frequency, the angle θ also varies with respect to the frequency, thereby enabling the frequency-dependent beam scanning. Such property is useful in many wireless systems that require the beam scanning function, as it does not need complex feeding networks and phase shifters used in conventional phased arrays. Eq. (9) also indicates that an ideal backfire-to-endfire ($-90°$ to $+90°$) radiation may be possible, provided that the propagation constant is properly engineered.

3. Free space scanning and adaptative CRLH LWAS

As discussed above, CRLH LWAs can exhibit frequency-dependent beam scanning capabilities for continuously varying the beam from backfire to endfire directions by frequency tuning. Using this unique property, novel tunable and adaptive LWAs can be realized [20–28]. This section will discuss the practice of MTM-based LWAs and the experimental demonstrations for free space scanning capability with enhanced functionality.

The radiation pattern of 1D CRLH LWA can be represented using the array factor approach, assuming the antenna is oriented along x-direction [18]:

$$AF(\theta) = \sum_{n=1}^{N} I_n e^{j(n-1)k_0 p_x \sin\theta - j\varphi_{xn}} \tag{10}$$

where N is the number of the CRLH unit cells, p_x is the periodicity of unit cells, $\varphi_{xn} = (n-1)k_0 p_x \sin\theta_{MB}$, $I_n = I_0 e^{-\alpha(n-1)p_x}$ is an exponentially decaying function determined by the leakage factor α. As β for CRLH TLs can vary from $-k_0$ to $+k_0$, the main beam of 1D CRLH LWA can scan continuously from θ = $-90°$ to $+90°$ ($-x$ to $+x$ direction) as indicated in (9).

A typical microstrip realization for a CRLH-TL using the printed circuit board (PCB) technology is shown in **Figure 7** [8]. The unit cell of the CRLH-TL contains an interdigital capacitor and a stub inductor to form the desired LH elements. The size of unit cell is much smaller than the guided wavelength such that the structure behaves as an effectively homogenized in the frequency range of interest. Assuming
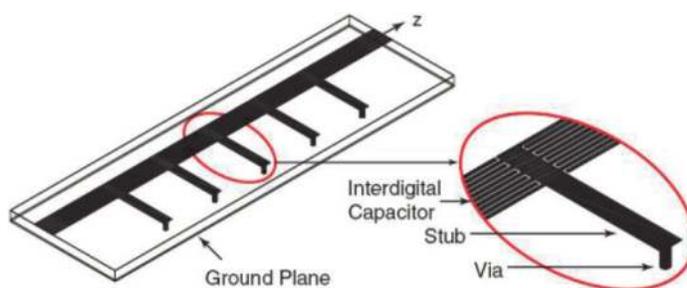
Figure 7.
Microstrip implementation of for a 1D CRLH-TL MTMstructure comprising periodically repeated sub-wavelength unit cells [8].

a lossless scenario, the unit cell model of this planar MTM TL can be described by the equivalent circuit in **Figure 3**. Owing to the inevitable parasitic effects, the right-handed series inductance and shunt capacitance need to be included, which forms an entire CRLH unit cell exhibiting a modal dispersion as shown in **Figure 4**: LH components dominate at lower frequencies, whereas RH components dominate at higher frequencies. A more rigorous unit cell model should also take into account the radiation loss (leakage rate), which are associated with resistance R and conductance G in the TL circuit model [15]. It is worth mentioning that the characteristic impedance is nearly independent of frequency for both RH and LH operations if properly designed, allowing a broadband impedance matching (i.e., 50 Ω in most RF and microwave systems).

Figure 8 shows a 24-cell CRLH LWA prototype and the measured radiation pattern. It is evident that as the frequency increases, the main beam direction scans from backward to forward, achieving a one-dimensional frequency scanning [5]. Ideally, a CRLH LWA scans a broad range of spatial region from $-90°$ to $+90°$, as frequency varies from $\omega = \beta \cdot c$ to $\omega = +\beta \cdot c$, including the broadside direction ($\theta = 0°$), which is usually at the evanescent mode for conventional LWAs [17].

In order to perform 2D frequency scanning, the antenna array must scan along another orthogonal direction, that is, y-direction as well. This can be achieved by properly designing the delay lines to manipulate the phase responses of each
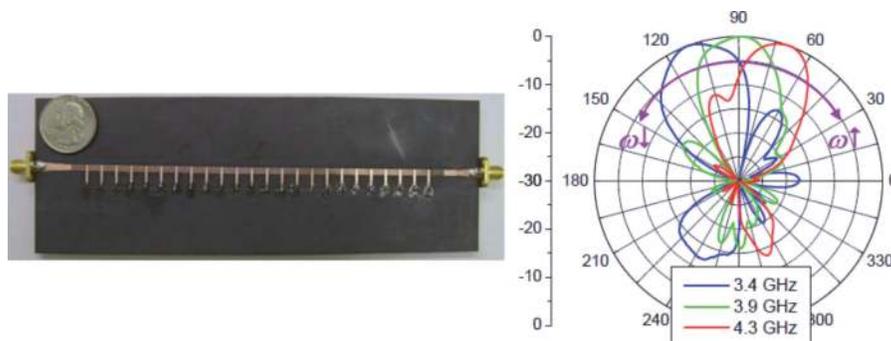
Figure 8.
*Prototype of **Figure 7** and its measured radiation patterns for different operating frequencies [8].*
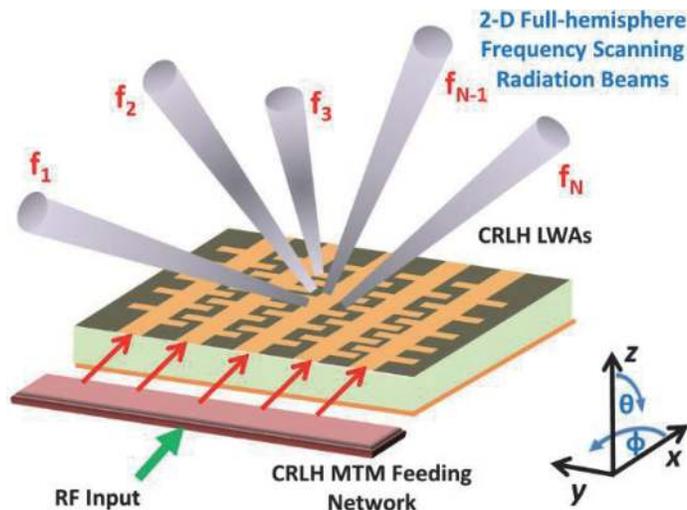
Figure 9.
Schematic of the proposed 2D MTM frequency scanning array exhibiting one-to-one frequency-space mapping [29].
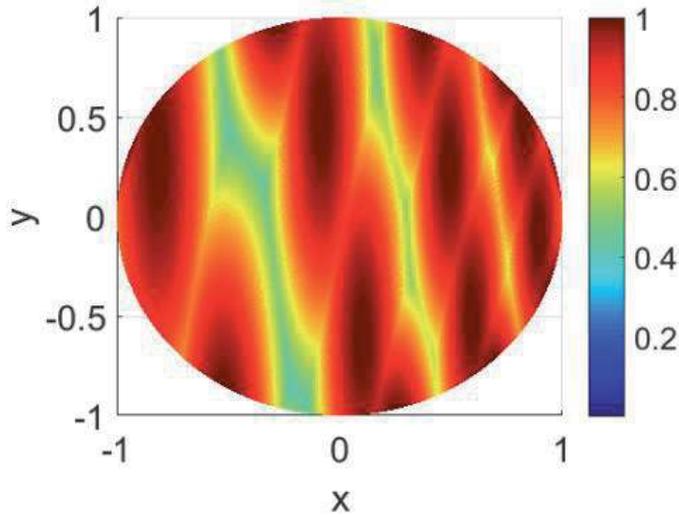
Figure 10.
Theoretical radiation beams using 2D array factor approach in (13) with L = 32, M = 2, N = 20. The frequency sweeps from 3 to 6.2 GHz, with an interval of 200 MHz, while each of the main beams corresponds to a distinct frequency [29].
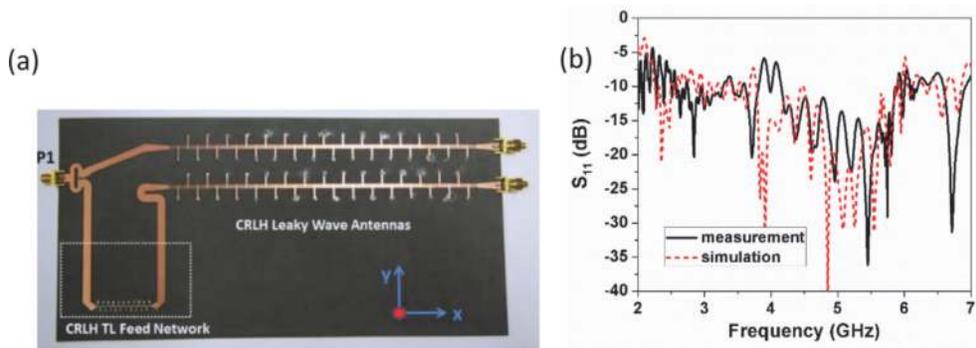
Figure 11.
Prototype of the proposed 2D MTM frequency scanning array. Measured and simulated return loss of the antenna array [29].

antenna element. To illustrate, the main beam angle of a 1D phased array is a function of progressive phase shift ξ, and can be represented as [19, 30]:

$$\theta_{array}(\omega) = \sin^{-1}\left(\frac{\xi}{k_0 d}\right) \tag{11}$$

Nevertheless, conventional delay lines can only provide phase delay, which bounds the radiated beam angles to only half of the hemisphere. To this end, if CRLH-TLs are used as feeding structures, they are able to provide both phase advance and phase delay, while exhibiting a zero phase-shift at the center operating frequency. Combining the CRLH-based feed network with 1D CRLH LWAs, the resulting 2D CRLH array can perform a 2D frequency-space mapping scheme as illustrated in **Figure 9** [29].

To explain, the phase response of a balanced CRLH TL consisting of N cascaded unit cells can be expressed as

$$\phi_{CRLH}(\omega) = -N\omega\sqrt{L_R C_R} + \frac{N}{\omega\sqrt{L_L C_L}} \tag{12}$$

where L_R, C_R and L_L, C_L are right-handed inductance and capacitance, as well as left-handed inductance and capacitance of a CRLH unit cell. It is observed from (12) that both positive and negative phase delay can be achieved using the CRLH feeding structures with respect to the operating frequency. Furthermore, if the phase response of the CRLH feed network varies fast enough within each sub-band of CRLH LWAs, a sequential 2D frequency scanning can be realized.

(a) 3.0 GHz **(b) 3.2 GHz**

(c) 3.5 GHz **(d) 3.9 GHz**

(d) 4.1 GHz **(e) 4.8 GHz**

(f) 5.5 GHz **(g) 5.9 GHz**
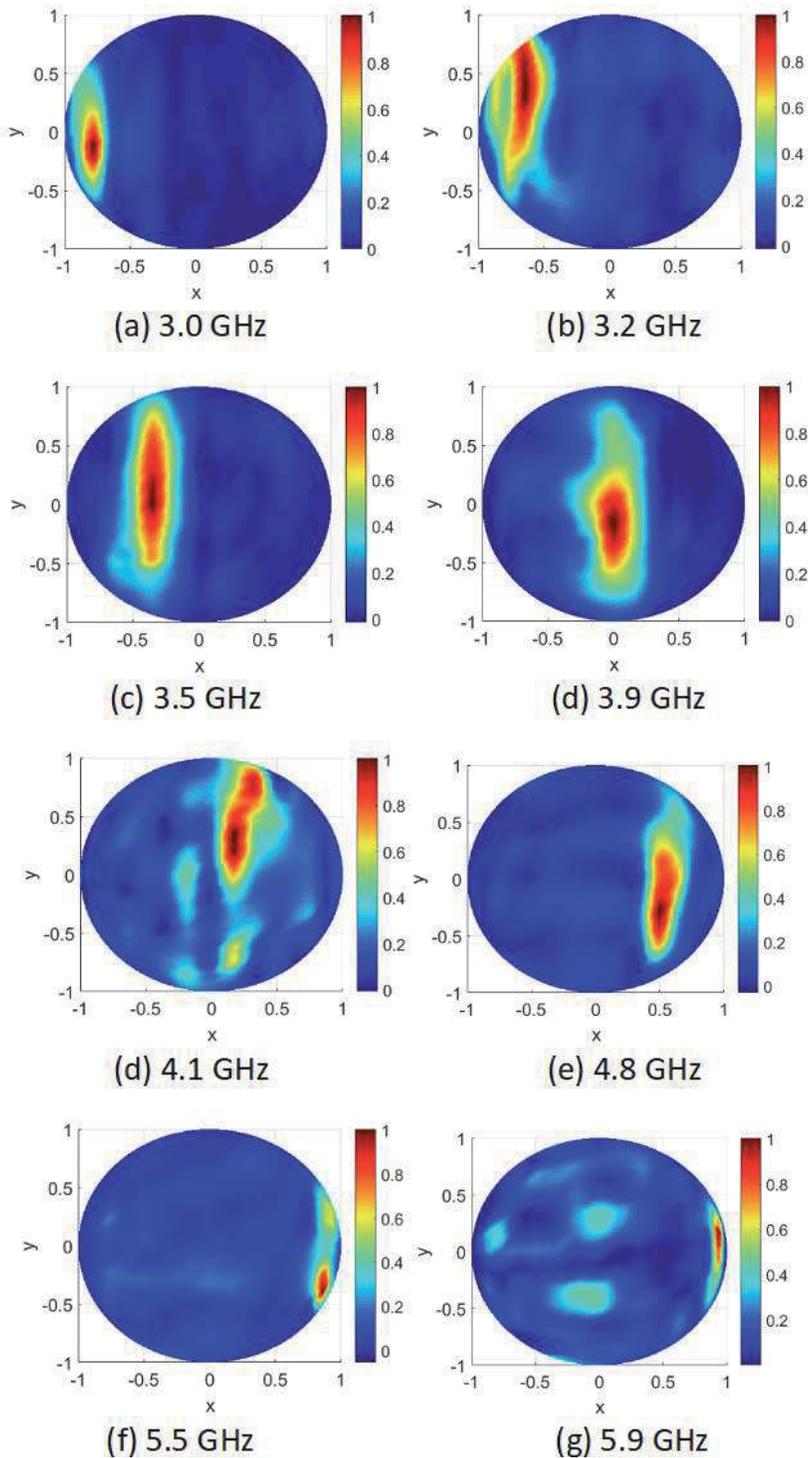
Figure 12.
Measured radiation patterns of the proposed 2D MTM frequency scanning array [29].

The 2D frequency scanning CRLH LWA array can be analyzed using the theoretical model based on 2D array factor approach. Its mathematical form is represented by the multiplication of the array factor of a 1D CRLH LWA and the one resulted from the phased array fed by the CRLH feed networks:

$$AF(\theta, \phi) = \sum_{n=1}^{L} I_n e^{j(n-1)k_0 p_x \sin\theta \cos\phi - j\varphi_{xn}} \times \sum_{m=1}^{M} e^{j(m-1)k_0 p_y \sin\theta \sin\phi + j\varphi_{yn}} \qquad (13)$$

where L is the number of the unit cells for a CRLH LWA, p_x is the periodicity of LWA unit cells, $\varphi_{xn} = (n-1)k_0 p_x \sin\theta_{MB}$, $I_n = I_0 e^{-\alpha(n-1)p_x}$ is an exponentially decaying function determined by the leakage factor α. Moreover, p_y is the spacing between the CRLH LWAs, M is the number of LWAs and $\varphi_{yn} = (m-1)\left(-N\omega\sqrt{L_R C_R} + \frac{N}{\omega\sqrt{L_L C_L}}\right)$, which is the phase response of CRLH feed lines with N unit cells.

For proof-of-concept, the CRLH LWA is designed to operate at 3–6.2 GHz. **Figure 10** plots the results of 2D MTM array obtained from (13) with a 200 MHz sweeping interval. For simplicity, the spatial location and radiation intensity are both normalized, where $x = \sin\theta\cos\phi, y = \sin\theta\sin\phi$. As a result, the resulting 2D CRLH aperture exhibit one-to-one frequency-space mapping characteristics covering the entire hemisphere above the radiating aperture, with each spectral component pointing to a specific angle in the free space.

To verify, a prototype of 2D MTM LWA array using printed circuit board (PCB) technology is shown in **Figure 11a**. The antenna array prototype contains two CRLH LWAs and a lumped component-based CRLH feed network embedded in a Wilkinson power divider. The return loss of the proposed structure is shown in **Figure 11b**. The measured results agree reasonably well with the EM simulation using ANSYS Electronics, indicating a good return loss within the operating band of 3–6.2 GHz. The slight mismatch at the center frequency around 4 GHz might be due to the handmade fabrication errors.

The measured radiation patterns of various frequencies within the antenna operating band are plotted in **Figure 12**. As can be seen, the main beam of the 2D
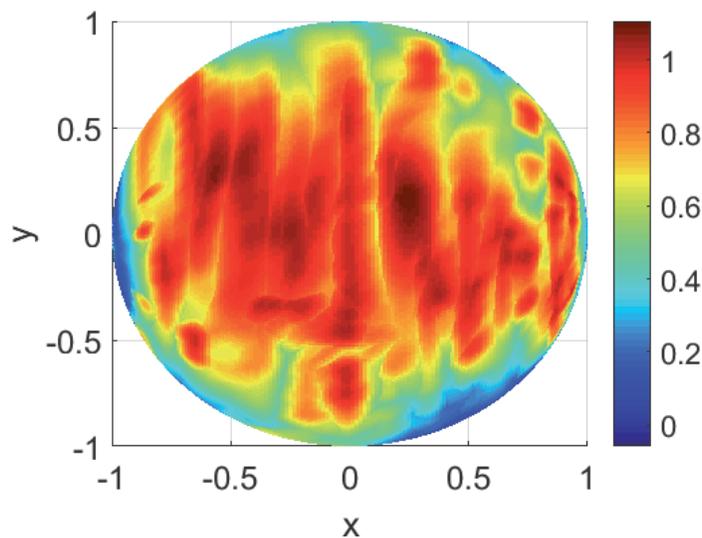
Figure 13.
Measured overlaid radiation beams of the fabricated 2D MTM array sweeping from 3 to 6.2 GHz with 25 MHz frequency steps [29].

MTM array is able to sweep in two dimensions, namely x-direction and y-direction. The x-direction scanning is due to the nature of CRLH LWAs, whereas the y-direction scanning results from the CRLH feed network that provides the required progressive phases. This mechanism leads to 2D frequency-to-space mapping capability. In addition, **Figure 13** overlays all the radiation patterns of the entire operating band from 3 to 6.2 GHz with an interval of 25 MHz. It can be observed that the main beams are frequency-mapped to the entire 2D full-hemisphere space.

4. Beamforming based on planar metasurfaces

This section discusses a new type of holographic antenna using the ultralow-profile metasurface hologram. Similar to the concept of transformation optics using MTMs, radiation from the metasurface relies on transforming the guided surface wave into the free-space radiation leakage, through its interactions with the anisotropic reactance tensor of metasurface defined by the analytical formula. The metasurface with an inhomogeneous and anisotropic surface impedance profile can be implemented using dense, textured subwavelength metallic structures printed on a printed circuit board. The beam angle with respect to the propagation direction of the surface wave depends on the spatial profile of surface impedance of the metasurface. Like the TL-MTM antenna, the metasurface antennas can be built with the standard PCB process and be excited by a simple in-plane feeder or a plane wave excitation. Therefore, the metasurface-based holographic antennas show significant potential for making compact, low-profile and conformal surface-like antennas, which have capabilities of generating a high-gain and steerable beam for satellite and space applications. Unlike the transformation optics approaches based on bulky MTMs [27, 28, 31, 32], where the control on propagation often requires highly anisotropic values for $\bar{\bar{\varepsilon}}$ and $\bar{\bar{\mu}}$ tesnors, the applicability of transformation techniques to 2D metasurface can avoid the complex transformation structures, power losses and manufacturing cost.

A metasurface can be seen as a 2D version of metamaterial, which is formed by arranging subwavelength scatters or apertures into a surface or interface [33–35]. Through the design of size, period and shape of textured surface, the metasurface can display a quasi-homogeneous or anisotropic surface impedance profile [34–38]. For many applications, metasurfaces have been be used in place of bulky MTMs because they occupy less physical space, reducing remarkably the manufacturing cost, and providing lower power loss and broader bandwidth when compared with their MTM counterparts. Metasurfaces have been exploited to make novel electromagnetic devices with superior performance and compactness [33]. The metasurface concept has emerged as an advantageous reconfigurable antenna architecture for beam forming and wave-front shaping. Metasurface antennas consist of an array of subwavelength inclusions (meta-atoms) distributed over an electrically large structure. In this section, we will discuss recent research advances in metasurfaces, which bring new exciting applications in RF and microwave beamforming technologies. Particularly, using the reconfigurable metasurface in conjunction with the holography principle enables new types of holographic antennas that electronically steer the beam, with a high realized gain and a low sidelobe level.

4.1 Principle of holographic antennas

Holographic antennas are a class of antennas whose radiation apertures are formed by the discrete spatially distributed diffraction apertures. As inspired by the

optical holography, the surface impedance profile of such an inhomogeneous planar aperture can be generated by the interference pattern of the desired (signal) beam with that of the reference beam. The concept of microwave holography or holographic antenna was first demonstrated by Checcacci, Russo and Scheggi in 1970 [39]. Microwave holographic antennas have been widely investigated in the past decades [40]. Typically, microwave holographic antennas typically comprise a main surface-wave-carrying impedance surface, which is separated from the ground plane by a dielectric slab. Such an impedance surface can be designed to serve as a guiding structure or to support leaky waves, depending on the eigenmodes of the surface-wave structure and/or the modulation period and depth of equivalent surface impedance [39–46]. The pattern of surface perturbations and spatial profile of surface impedance can be designed by a "holography" method [41]. In this context, the electrically thin metasurface has been known for its capabilities of controlling the phase and amplitude fronts of surface waves [40–48]. As a result, metasurfaces may serve as an ideal platform for microwave holograms that gives control to the amplitude, phase and polarization of aperture fields.

The holography process involves producing an interference pattern using two waves, and then using the interference pattern to scatter one wave to produce the other. The interference pattern formed by these two waves is recorded as a *hologram*. When the reference wave illuminates the hologram, it is scattered by the recorded interference pattern to produce a copy of the original object wave. For a reference wave Ψ_{ref} and an object wave Ψ_{obj}, the interference pattern contains a term proportional to $\Psi_{obj}\Psi_{ref}^*$. When the interference pattern is illuminated by the reference wave, it renders $\left(\Psi_{obj}\Psi_{ref}^*\right)\Psi_{ref} = \Psi_{obj}\left|\Psi_{ref}\right|^2$, forming a copy of the original object wave. For the case of a leaky-wave antenna excited by the bound transverse magnetic (TM) surface modes, we may define the geometrical surface perturbation as the interference pattern between these two waves [41]:

$$Z(x,y) = j\left|X + M \ \text{Re}\left[\Psi_{rad}\Psi_{ref}^*\right]\right|, \tag{14}$$

where X and M are the arbitrary real average value and the real modulation depth at the position (x,y) on the impedance surface; we assume the surface lies in the x-y plane. The radiated (object) wave can be seen as the product of surface-wave scattering from a modulated surface, given by $\Psi_{obj}\left|\Psi_{ref}\right|^2$.

For the one-dimensional applications (**Figure 14**), the hologram is produced by the interference pattern of a 1D surface wave and a plane wave propagating in free space at an θ_0 Sampling the hologram impedance function at each unit cell center gives the local impedance value and hence the geometry and size of local metal patch.

In principle, generation of arbitrary polarization requires an anisotropic and inhomogeneous metasurface. Consider a uniform and anisotropic metasurface lies on the x-y plane, the averaged tangential electric field at the surface $\overline{\mathbf{E}}\big|_{z=0^+}$ is related to the averaged induced surface current $\overline{\mathbf{J_s}}$ by $\overline{\mathbf{E}}\big|_{z=0^+} = \overline{\overline{\mathbf{Z}}} \cdot (\hat{z} \times \overline{\mathbf{H}})\big|_{z=0^+} = \overline{\overline{\mathbf{Z}}} \cdot \overline{\mathbf{J_s}}$, where the surface impedance dyad $\overline{\overline{\mathbf{Z}}}$ appearing in a tensor form is given by [41, 42]:

$$\begin{pmatrix} E_x \\ E_y \end{pmatrix} = \begin{pmatrix} Z_{xx} & Z_{xy} \\ Z_{yx} & Z_{yy} \end{pmatrix} \begin{pmatrix} J_x \\ J_y \end{pmatrix} \tag{15}$$

In the lossless scenario, the surface impedance tensor $\overline{\overline{\mathbf{Z}}}$ is anti-Hermitian (i.e., $\overline{\overline{\mathbf{Z}}} = -\overline{\overline{\mathbf{Z}}}^{*T}$), and the applicability of reciprocity enforces that $\overline{\overline{\mathbf{Z}}}$ is purely imaginary
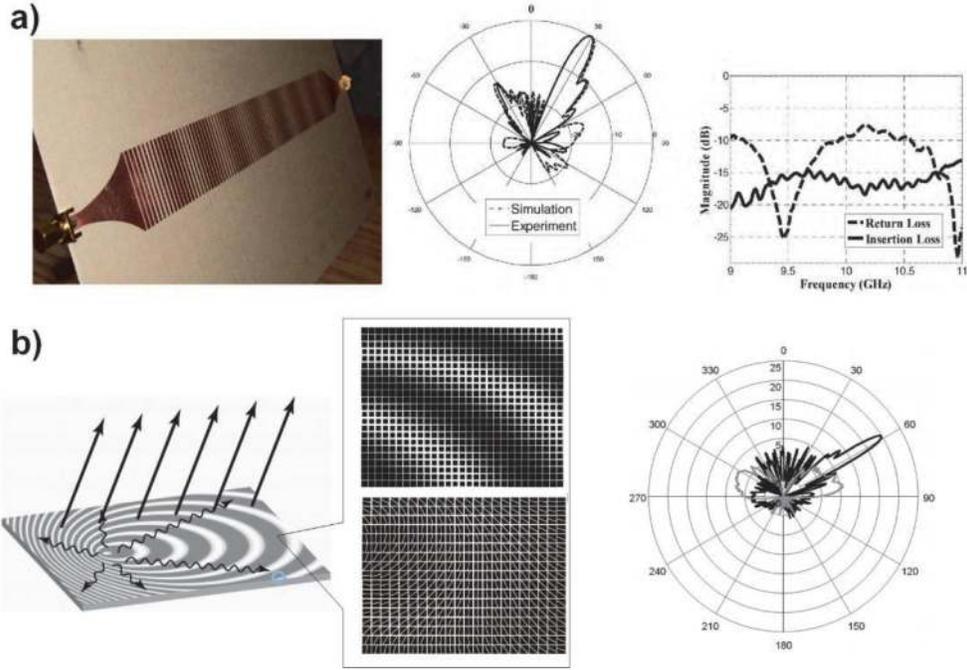
Figure 14.
(a) Left: 1D holographic leaky wave antenna using a metasurface composed of a subwavelength metal strips on top of a grounded dielectric substrate. The local surface reactance is varied by adjusting the strip width. Right: Measured radiation patterns and bandwidth of operation [43]. (b) 2D holographic leaky wave antenna using a metasurface and a zoomed-in hologram portion and unit cells (metallic patch of different geometric shapes that are printed on top of a grounded dielectric substrate). The undulating and straight arrows represent the surface wave and desired radiation, respectively. The unit cell size is fixed at 3 mm, which is much smaller than the free space wavelength. Measured radiation patterns from a 3 mm monopole antenna placed above the holographic metasurface (black) and an untextured metal surface (gray) at 17 GHz. The inclination angle is defined from the impedance surface normal, that is, the z-axis in the x-z plane [42].

and $Z_{xy} = Z_{yx}$. The surface impedance tensor is constructed from the outer product of the expected surface current vectors and the desired outgoing electric field vectors. The outer product generalizes the simple multiplicative scalar pattern described earlier in this section. In the tensor case, the desired radiated vector wave term $\overline{\overline{\mathbf{E}}}_{rad} \left| \overline{\mathbf{J}}_{surf} \right|^2$ is obtained from scattering of a vector surface wave from a modulated anisotropic impedance surface with $\overline{\overline{\mathbf{Z}}}$. When the anisotropic metasurface hologram is illuminated with the reference surface wave, a modulated tensor impedance proportional to $\overline{\overline{\mathbf{E}}}_{rad} \otimes \overline{\mathbf{J}}_{surf}^{\dagger}$ can create a radiated vector wave term: $\overline{\overline{\mathbf{Z}}} \cdot \overline{\mathbf{J}}_{surf} \propto \overline{\mathbf{E}}_{rad} \otimes \overline{\mathbf{J}}_{surf}^{\dagger} \cdot \overline{\mathbf{J}}_{surf} = \overline{\mathbf{E}}_{rad} \cdot \left| \overline{\mathbf{J}}_{surf} \right|^2$ (the dagger represents the Hermitian conjugate). For a power-conserving and reciprocal metasurface, $\overline{\overline{\mathbf{Z}}}$ must be made anti-Hermitian and pure imaginary, given by:

$$\overline{\overline{\mathbf{Z}}} = j \begin{pmatrix} X & 0 \\ 0 & X \end{pmatrix} + j \frac{M}{2} \mathrm{Im}\left[\overline{\mathbf{E}}_{rad} \otimes \overline{\mathbf{J}}_{surf}^{\dagger} - \overline{\mathbf{J}}_{surf} \otimes \overline{\mathbf{E}}_{rad}^{\dagger} \right] \qquad (16)$$

where the diagonal X in the impedance matrix binds the TM surface wave, and the modulated impedance components M scatter the vector surface wave into the desired vector outgoing wave. A circularly polarized planar antenna using the anisotropic holographic metasurface have been demonstrated in Ref. [44], of which the circularly polarized radiation is produced from a linearly polarized source through interactions with the transformative metasurface hologram.

The metasurface-based holographic antenna can be made extremely flat, light weight (<1 kg), low cost and built with the standard PCB processes. Since each elementary inclusion on the metasurface is subwavelength and non-resonant, this holographic antenna exhibits satisfactory insertion and return losses.

With the advent in the metasurface technology, one already has the ability to accurately define the local surface impedance profile of metasurface and conduct the inverse design of the spatially invariant inclusions over the surface. Several approaches have been proposed to design and characterize the surface impedance dyad of metasurfaces with great accuracy [48]. **Figure 15** shows a prototype of circularly polarized holographic antenna based on an anisotropic metasurface [44]. To produce the anisotropic impedance, the geometry of metallic patch must be asymmetric with respect to the propagation direction of the surface wave. The measured realized gain in the horizontal plane at 8.6 GHz is also presented in **Figure 15**. It is clearly seen that the metasurface-based holographic antenna exhibits an excellent contrast between the right-handed circular-polarization radiation (co-polarization) and left-handed circular-polarization radiation (cross-polarization) radiation. Noticeably, a broadband and broad-angle operation could be achieved with this compact metasurface antenna.

Combining the holography concept with the reconfigurable metasurface will further allow dynamic beamsteering capabilities, without the need of mechanical moving parts [49–57]. In 2013, the Kymeta Corporation has demonstrated an active metasurface antenna used for bi-directional high-speed internet connectivity [49]. In their design, the reconfigurability is achieved by using inclusions (i.e., meta-atoms) that can be individually tuned to create a dynamic hologram. In their design, controlling local radiative responses is possible by loading each meta-atom with liquid crystals that present a variable permittivity tensor. Moreover, a dynamic hologram with faster response time and lower loss may be achieved by exploiting meta-atoms loaded with active electronic components (e.g., transistors or diodes).
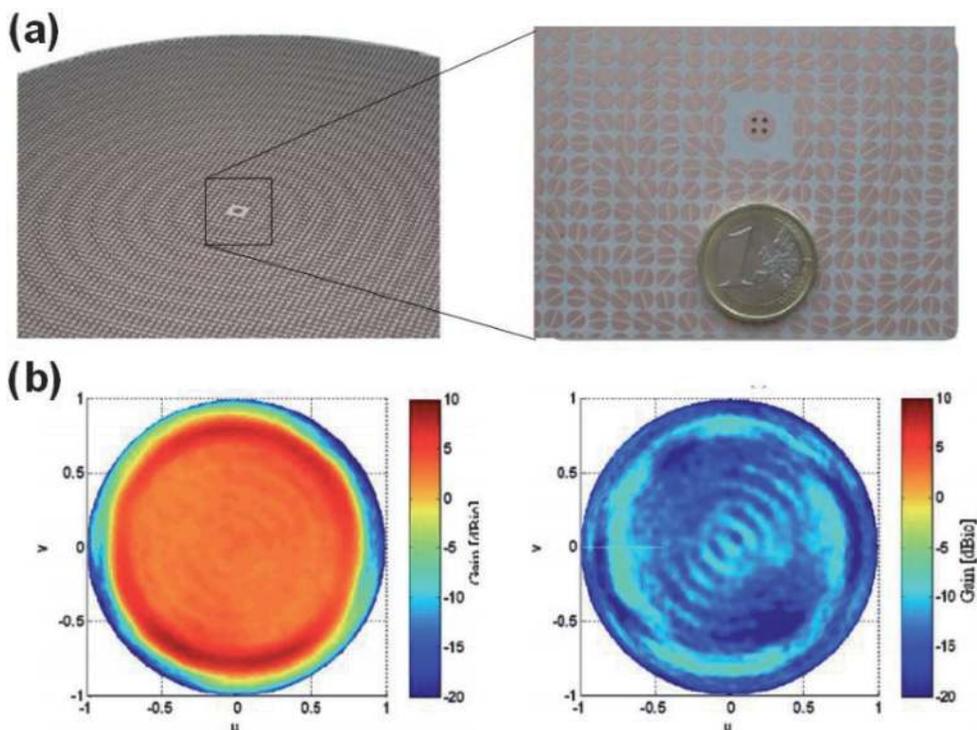
Figure 15.
(a) Photograph of the prototype of circularly polarized metasurface antenna and details of its feeding zone without exciter pin. (b) Gain measurements for the antenna at 8.6 GHz on the horizontal plane: (left) RHCP component and (right) LHCP component [44].
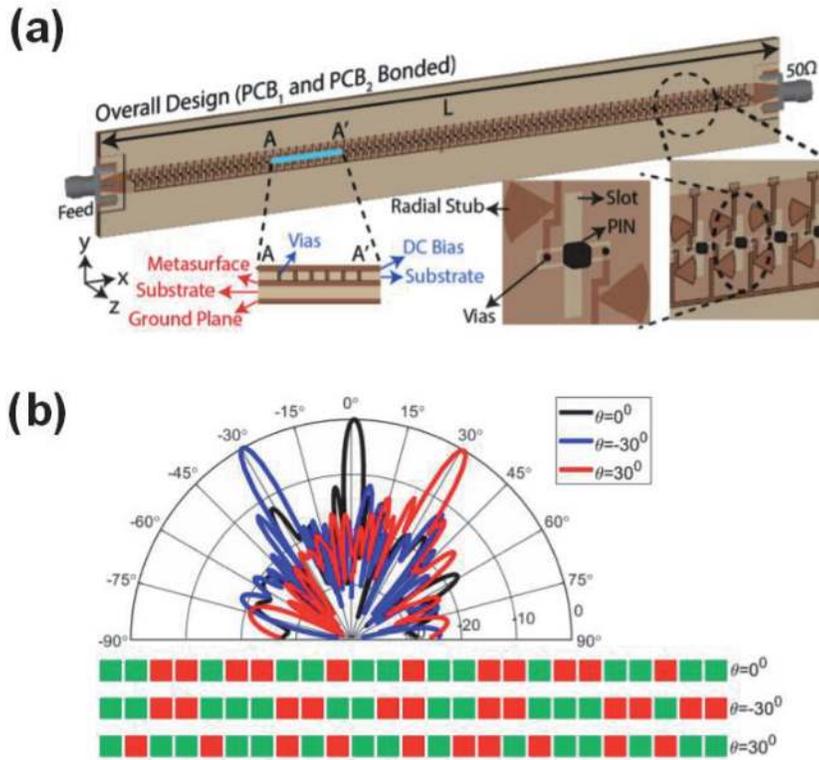
Figure 16.
Reconfigurable metasurface made of arrays of meta-atom apertures loaded with PIN diodes [51]. A tunable metasurface antenna: the input carrier wave traverses the waveguide and the meta-atom couple energy out of the feed; an unit cell is switched to its on- and off-states by the external circuitry. (b) When this holographic antenna is illuminated by an underlying feed wave, a coherent beam is produced. Different images, encoded in the array by the control circuit, produce various radiations over a broad angular range.

Ideally, each meta-atom must be weakly coupled and be capable of being individually driven to obtain different electromagnetic properties at the scale of a single unit cell. Enhancement of bandwidth is also possible by combining metasurfaces with non-Foster elements. Different from conventional phase arrays and leaky-wave antennas, a dynamic metasurface antenna does not require active phase shifters and amplifiers, and can achieve reconfigurability locked to specific operating frequencies variant from 8.5 to 8.8 GHz.

Figure 16 shows schematically a reconfigurable holographic antenna based on the active metasurface, of which an individual unit cell is loaded with active component to vary the hologram pattern and thus change angular distributions of radiation. Modeling the collective responses from meta-atoms and the subsequent radiation pattern have been studied using the array factor method and the Dyadic Green's functions for dipole excitations [53, 56]. In addition, the analytical model for design of meta-atoms of different kinds can be found in [54]. Since each meta-atom can be modeled as a polarizable dipole, its polarizability and radiative properties can be well defined. These modeling technique and the holographic explanation shed light on important considerations for achieving an better control of radiation patterns produced by the active metasurface antenna [50–55].

5. Conclusions

Planar MTM technologies manipulating the electromagnetic waves, somehow similar to the transformation optics, may suggest new types of efficient

beamforming and beamshaping techniques for the modern wireless systems. This chapter has presented some of the most recent and representative innovations in the planar TL-MTMor metasurface antenna based on the microstrip implementation. Their operation principles basically rely on tailoring the propagation (phase) constant and impedance by using the homogenized, subwavelength reactive elements in an effective medium. Further, the tunability in phase velocity, propagation constant and impedance can be achieved with the combinational responses associated with the periodic nature of metamaterial/metasurface structure and with the loaded lumped components (i.e., diodes, varactors, switches and transistors) in the unit cell. This enables the beamforming and beamsteering antennas to be made thinner, lighter weight, less expensive and requiring less power and having enhanced bandwidth than the conventional alternatives; for instance, phase arrays typically include multiple active antennas with costly phase shifters, amplifiers and complex feeding structures. The novel surface antenna technologies, being capable of dynamically transforming the guided waves to the desired radiation patterns, show great potential to serve as beamformers and beamsteerers for the next-generation wireless technology [58, 59].

Author details

Chung-Tse Michael Wu[1*] and Pai-Yen Chen[2]

1 Department of Electrical and Computer Engineering, Rutgers, The State University of New Jersey, NJ, USA

2 Department of Electrical and Computer Engineering, University of Illinois at Chicago, Chicago, IL, USA

*Address all correspondence to: ctm.wu@rutgers.edu

IntechOpen

References

[1] Sihvola A. Metamaterials in electromagnetics. Meta. 2007;**1**(1):2-11

[2] Smith DR, Padilla WJ, et al. Composite medium with simultaneously negative permeability and permittivity. Physical Review Letters. 2000;**84**(18): 4184-4187

[3] Shelby RA, Smith DR, et al. Experimental verification of a negative index of refraction. Science. 2001; **292**(5514):77-79

[4] Yen TJ, Padilla WJ, et al. Terahertz magnetic response from artificial materials. Science. 2004;**303**(5663):1494

[5] Caloz C, Itoh T. Electromagnetic Metamaterials: Transmission Line Theory and Microwave Applications. Hoboken, New Jersey: John Wiley & Sons; 2005

[6] Eleftheriades GV, Iyer AK, Kremer PC. Planar negative refractive index media using periodically LC loaded transmission lines. IEEE Transactions on Microwave Theory and Techniques. 2002;**50**(12):2702-2712

[7] Engheta N, Ziolkowski RW, editors. Metamaterials: Physics and Engineering Explorations. Hoboken, New Jersey: John Wiley & Sons; 2006

[8] Lai A, Itoh T, Caloz C. Composite right/left-handed transmission line metamaterials. IEEE Microwave Magazine. 2004;**5**(3):34-50

[9] Kuylenstierna D, Vorobiev A, Linner P, Gevorgian S. Composite right/ left handed transmission line phase shifter using ferroelectric varactors. IEEE Microwave and Wireless Components Letters. 2006;**16**(4):167-169

[10] Tseng CH, Itoh T. IEEE MTT-S International Microwave Symposium Digest. IEEE; 2006. pp. 931-934

[11] Eleftheriades GV, Grbic A, Antoniades M. Negative-refractive-index transmission-line metamaterials and enabling electromagnetic applications. In: IEEE APS-S International Antennas and Propagation Society International Symposium. IEEE; 2004. pp. 1399-1402

[12] Eleftheriades GV. EM transmission line metamaterials. Materials Today. 2009;**12**(3):30-41

[13] Liu L, Caloz C, Itoh T. Dominant mode leaky-wave antenna with backfire-to-endfire scanning capability. Electronics Letters. 2002;**38**(23): 1414-1416

[14] Allen CA, Leong KM, Itoh T. 2-D frequency-controlled beam-steering by a leaky/guided-wave transmission line array. In: IEEE MTT-S International Microwave Symposium Digest. IEEE; June 2006. pp. 457-460

[15] Lim S, Caloz C, Itoh T. Metamaterial-based electronically controlled transmission-line structure as a novel leaky-wave antenna with tunable radiation angle and beamwidth. IEEE Transactions on Microwave Theory and Techniques. 2004;**52**(12): 2678-2690

[16] Casares-Miranda FP, Camacho-Peñalosa C, Caloz C. High-gain active composite right/left-handed leaky-wave antenna. IEEE Transactions on Antennas and Propagation. 2006;**54**(8): 2292-2300

[17] Oliner AA. In: John RC, editor. Leaky-Wave Antennas. Antenna Engineering Handbook. 3rd ed. New York, New York: McGraw-Hill; 1993

[18] Caloz C, Itoh T. Array factor approach of leaky-wave antennas and application to 1-D/2-D composite right/left-handed (CRLH) structures.

IEEE Microwave and Wireless Components Letters. 2004;**14**(6): 274-276

[19] Choi J, Sun JS, Itoh T. Frequency-scanning phased-array feed network based on composite right/left-handed transmission lines. IEEE Transactions on Microwave Theory and Techniques. 2013;**61**(8):3148-3157

[20] Huang L, Chiao J, Lisio P. An electronically switchable leaky wave antenna. IEEE Transactions on Antennas and Propagation. 2000; **48**(11):1769-1772

[21] Maheri H, Tsutsumi M, Kumagi N. Experimental studies of magnetically scannable leaky-wave antennas having a corrugated ferrite slab/dielectric layer structure. IEEE Transactions on Antennas and Propagation. 1988;**36**(7): 911-917

[22] Wu C-TM, Dong Y, Sun JS, Itoh T. Ring-resonator-inspired power recycling scheme for gain-enhanced distributed amplifier-based CRLH-transmission line leaky wave antennas. IEEE Transactions on Microwave Theory and Techniques. 2012;**60**(4): 1027-1037

[23] Wu C-TM, Itoh T. Combined gain-enhanced power recycling feedbacks for distributed amplifier-based crlh-leaky wave antennas. In: 41st European Microwave Conference (EuMC). IEEE; 2011. pp. 499-502

[24] Wu C-TM, Itoh T. Gain-enhanced distributed amplifier-based CRLH-leaky wave antenna for quasi-resonant power recycling scheme. In: Microwave Symposium Digest (MTT). IEEE; 2011. pp. 1-4

[25] Wu C-TM, Itoh T. Dual-fed distributed amplifier-based CRLH-leaky wave antenna for gain-enhanced power combining. In: IEEE MTT-S International Microwave Workshop

Series on Innovative Wireless Power Transmission - Technologies, Systems, and Applications (IMWS). IEEE; 2012, May. pp. 87-90

[26] Wu C-TM, Itoh T. CRLH-transmission line leaky wave antennas integrated with distributed amplifiers with power recycling feedback scheme. In: Proceedings of the 5th European Conference on Antennas and Propagation (EUCAP). IEEE; April 2011. pp. 3901-3904

[27] Pendry JB, Schurig D, Smith DR. Controlling electromagnetic fields. Science. 2006;**312**(5781):1780-1782

[28] Leonhartdt U. Optical conformal mapping. Science. 2006;**312**(5781): 1777-1780

[29] Salarkaleji M, Ali MA, Wu C-TM. Two-dimensional full-hemisphere frequency scanning array based on metamaterial leaky wave antennas and feed networks. In: IEEE MTT-S International Microwave Symposium (IMS). IEEE; 2016. pp. 1-4

[30] Stutzman W, Thiele GA. Antenna Theory and Design. Hoboken, New Jersey: John Wiley & Sons; 2012

[31] Chen H, Chan CT, Sheng P. Transformation optics and metamaterial. Nature Materials. 2010;**9**: 387-396

[32] Ma HF, Cui TJ. Three-dimensional broadband and broad-angle transformation-optics lens. Nature Communications. 2010;**1**:124

[33] Holloway CL, Kuester EF, et al. An overview of the theory and applications of metasurfaces: The two-dimensional equivalents of metamaterials. IEEE Antennas and Propagation Magazine. 2012;**54**(2):10-35

[34] Holloway CL, Mohamed MA, et al. Reflection and transmission properties

of a metafilm: With an application to a controllable surface composed of resonant particles. IEEE Transactions on Antennas and Propagation. 2005;**47**(4): 853-865

[35] Holloway CL, Kabos P, et al. Realization of a controllable metafilm/metasurface composed of resonant magnetodielectric particles: Measurements and theory. IET Microwaves, Antennas and Propagation. 2010;**4**(8):1111-1122

[36] Chen PY, Alù A. Mantle cloaking using thin patterned metasurfaces. Physical Review B. 2011;**84**(20):205110

[37] Padooru YR, Yakovlev AB, Chen PY, Alù A. Analytical modeling of conformal mantel cloaks for cylindrical objects using sub-wavelength printed and slotted arrays. Journal of Applied Physics. 2012;**112**(3):034907

[38] Padooru Y, Yakovlev R, Chen PY, Alù A. Line-source excitation of realistic conformal metasurface cloaks. Journal of Applied Physics. 2012;**112**(10): 104902

[39] Checcacci P, Russo V, Scheggi A. Holographic antennas. IEEE Transactions on Antennas and Propagation. 1970;**18**(6):811-813

[40] ElSherbiny M, Fathy AE, et al. Holographic antenna concept, analysis and parameters. IEEE Transactions on Antennas and Propagation. 2004;**52**(3): 830-839

[41] Fong BH, Colburn JS, et al. Scalar and tensor holographic artificial impedance surfaces. IEEE Transactions on Antennas and Propagation. 2010; **58**(10):3212-3221

[42] Sievenpiper D, Colburn J, et al. Holographic artificial impedance surfaces for conformal antennas. In: Antennas and Propagation Society International Symposium. IEEE; 2005. pp. 256-259

[43] Patel AM, Grbic A. A printed leaky-wave antenna based on a sinusoidally-modulated reactance surface. IEEE Transactions on Antennas and Propagation. 2011;**59**(6):2087-2096

[44] Minatti G, Maci S, et al. A circularly-polarized isoflux antenna based on anisotropic metasurface. IEEE Transactions on Antennas and Propagation. 2012;**60**(11):4998-5009

[45] Minatti G, Caminita F, et al. Spiral leaky-wave antennas based on modulated surface impedance. IEEE Transactions on Antennas and Propagation. 2011;**59**(12):4436-4444

[46] Chen PY, Farhat M, et al. Infrared beam-steering using acoustically modulated surface plasmons over a graphene monolayer. Journal of Optics. 2014;**16**(9):094008

[47] Eleftheriades GV, Wong AMH. Holography-inspired screens for sub-wavelength focusing in the near field. IEEE Microwave and Wireless Components Letters. 2008;**18**(4): 236-238

[48] Patel AM, Grbic A. Transformation electromagnetics devices using tensor impedance surface. In: MTT-S International Microwave Symposium Digest (IMS). IEEE; 2013. pp. 1-4

[49] Bleicher A. Kymeta Demos First Ever Satellite Link with Metamaterial Antenna. New York: IEEE Spectrum; 2013

[50] Johnson M, Bowen P, et al. Discrete-dipole approximation model for control and optimization of a holographic metamaterial antenna. Applied Optics. 2014;**53**(25):5791-5799

[51] Yurduseven O et al. Dynamically reconfigurable holographic metasurface aperture for a Mills-cross monochromatic microwave camera. Optics Express. 2018;**26**(5):5281-5291

[52] Yurduseven O et al. Millimeter-wave spotlight imager using dynamic holographic metasurface antennas. Optics Express. 2017;**25**(15): 18230-18249

[53] Smith DR et al. Analysis of a waveguide-fed metasurface antenna. Physical Review Applied. 2017;**8**(5): 054048

[54] Pulido-Mancera L et al. Polarizability extraction of complementary metamaterial elements in waveguides for aperture modeling. Physical Review B. 2017;**96**(23):235402

[55] Johnson M, Brunton SL, et al. Sidelobe canceling on a reconfigurable holographic metamaterial antenna. In: International Conference on Electromagnetics in Advanced Applications (ICEAA). 2014. pp. 806-809

[56] Lipworth G, Mrozack A, et al. Metamaterial apertures for coherent computational imaging on the physical layer. Journal of the Optical Society of America A. 2013;**30**(8):1603-1612

[57] Hunt J, Driscoll T, et al. Metamaterial apertures for computational imaging. Science. 2013; **339**(6117):310-313

[58] Mori K, Itoh T. Distributed amplifier with CRLH-transmission line leaky wave antenna. In: EuMC 2008. 38th European Microwave Conference. IEEE; 2008. pp. 686-689

[59] Wu C-TM, Itoh T. A re-radiating CRLH-transmission line leaky wave antenna using distributed amplifiers. In: APMC 2009. Asia Pacific Microwave Conference. IEEE; 2009. pp. 1998-2001